remote sensing

Article

GNSS RTK Positioning Augmented with Large LEO Constellation

Xingxing Li *, Hongbo Lv, Fujian Ma, Xin Li, Jinghui Liu and Zihao Jiang

School of Geodesy and Geomatics, Wuhan University, 129 Luoyu Road, Wuhan 430079, China; franktgreen@whu.edu.cn (H.L.); fjmasgg@whu.edu.cn (F.M.); lixinsgg@whu.edu.cn (X.L.); 2018282140133@whu.edu.cn (J.L.); 2014301610026@whu.edu.cn (Z.J.)

* Correspondence: lxlq109121@gmail.com

Received: 16 December 2018; Accepted: 18 January 2019; Published: 22 January 2019

Abstract: It is widely known that in real-time kinematic (RTK) solution, the convergence and ambiguity-fixed speeds are critical requirements to achieve centimeter-level positioning, especially in medium-to-long baselines. Recently, the current status of the global navigation satellite systems (GNSS) can be improved by employing low earth orbit (LEO) satellites. In this study, an initial assessment is applied for LEO constellations augmented GNSS RTK positioning, where four designed LEO constellations with different satellite numbers, as well as the nominal GPS constellation, are simulated and adopted for analysis. In terms of aforementioned constellations solutions, the statistical results of a 68.7-km baseline show that when introducing 60, 96, 192, and 288 polar-orbiting LEO constellations, the RTK convergence time can be shortened from 4.94 to 2.73, 1.47, 0.92, and 0.73 min, respectively. In addition, the average time to first fix (TTFF) can be decreased from 7.28 to 3.33, 2.38, 1.22, and 0.87 min, respectively. Meanwhile, further improvements could be satisfied in several elements such as corresponding fixing ratio, number of visible satellites, position dilution of precision (PDOP) and baseline solution precision. Furthermore, the performance of the combined GPS/LEO RTK is evaluated over various-length baselines, based on convergence time and TTFF. The research findings show that the medium-to-long baseline schemes confirm that LEO satellites do helpfully obtain faster convergence and fixing, especially in the case of long baselines, using large LEO constellations, subsequently, the average TTFF for long baselines has a substantial shortened about 90%, in other words from 12 to 2 min approximately by combining with the larger LEO constellation of 192 or 288 satellites. It is interesting to denote that similar improvements can be observed from the convergence time.

Keywords: real-time kinematic (RTK); LEO constellation augmented GNSS; medium-to-long baseline; convergence time; time to first fix (TTFF)

1. Introduction

With the fast development and widespread application of global navigation satellite system (GNSS), the demands of spatiotemporal information have already been changed from static to dynamic position, post to real-time process, and low to high precision. Currently, the real-time kinematic (RTK) positioning by using GNSS double-differenced (DD) observations can achieve centimeter-level positioning accuracy quickly after correctly performing the ambiguity resolution [1]. However, the RTK technique is limited to baseline length defined as the distance between the reference and rover stations, the main reason for which is that atmospheric activities above stations have an important influence on the DD ambiguity fixing [2]. For the short baselines with lengths usually shorter than 10 km, the remaining atmospheric delays, i.e., ionospheric and tropospheric delays can be significantly weakened or assumed negligible by forming DD observations, so that the carrier-phase ambiguities can be fixed correctly in short time, or even in one epoch [3]. On the other hand, the medium and long baselines with lengths up to tens or hundreds of kilometers, the remaining atmospheric errors, especially for ionospheric delays are hard to be eliminated by DD, which seriously affected the phase ambiguity fixing [4].

In order to solve this problem, there are many methods of addressing ionospheric residuals or improving ambiguity fixing within multiple frequencies or systems [5–9]. Odolinski et al. analyzed the instantaneous long-baseline RTK performance using the ionosphere-float strategy, based on dual-frequency GPS and BDS data [10]. The results have been shown that GPS+BDS scheme can significantly shorten the time to first fix (TTFF) from 21 to 12 min in comparison to the GPS scheme and thus quickly achieve ambiguity-fixed baseline precisions at the mm–m level. Meanwhile, it is also demonstrated that the combined system can accelerate convergence to reach a dm-level precision under the circumstance of the ambiguity-float solution. In addition, the multi-baseline network based RTK system can significantly mitigate atmospheric delays at the rover station by using generated spatial information, Gomi et al. investigated the relationship between the ionospheric effect and the scale of two medium networks from the aspects of positioning result and ambiguity success rate [11]. While in some case, such as the forest and urban environments, RTK technique cannot be good enough to deliver practical application [12,13]. Thanks to the appearance and development of low earth orbit (LEO) constellation with the orbit altitudes between 400 and 1500 km, which can provide much stronger signals against spoofing and jamming, as well as much faster movement speeds to improve satellites geometric distribution, compared with GNSS satellites [14,15]. Possibly, it will be an alternative or a complement for existing solutions to enhance the RTK positioning and navigation performance by combining GNSS and LEO satellites.

In recent years, some reliable data fusion algorithms utilizing LEO constellations to improve GNSS positioning performance have been under study. Back in the 1990s, Enge et al. explored a method and an apparatus which using LEO satellite signals to augment GPS differential positioning in a Trimble's patent [16]. Rabinowitz et al. designed a receiver which is capable of tracking GPS and Globalstar LEO satellites [17]. It is found that the ambiguity resolution could be achieved within 4 min by introducing Globalstar LEO constellation alone to short-range (1–5 km) differential positioning, which attributes to the improvement of geometric condition at ground stations. Afterwards, some researches about integrating the iridium and current GNSS measurements have been carried out to investigate the contribution of LEO augmentation, such as fulfilling navigation integrity requirements, revisiting nominal measurement error models, and accelerating floating ambiguities estimation [18,19]. Tian et al. examined the issue of rapid resolution of DD integer cycle ambiguities on short-baseline schemes by simulating an Iridium-like LEO constellation to augment GPS [20]. The result shows that higher ambiguity success rate and better ambiguity precision can be obtained through a hybrid MEO-LEO constellation scheme. Besides, more detailed simulation experiments and analyses have also been conducted to evaluate the performance of precise point positioning (PPP) with LEO constellation augmented GNSS [21–23]. Although there are many studies on the augmentation of LEO satellites, few experiments have been conducted on comprehensively investigating the medium- and long-range RTK performance.

In this paper, we focus on single-baseline RTK results using four kinds of LEO constellations in combination with GPS, all of which are based on the simulated pseudorange and carrier phase observations at ground tracking stations. The models considered for RTK in this work are divided into two types: short and medium-to-long baselines, which have been further introduced in Section 2, together with the simulation method of ground-based data. In Section 3, different constellation configurations, simulation situations, and data processing strategies are introduced, respectively, aiming to prepare for RTK positioning. After that the performances of different LEO constellations augmented GPS RTK are analyzed in Section 4 comprehensively. In Section 5, we will make an initial assessment of combined GPS/LEO RTK for different length baseline at mid-latitudes. Finally, the conclusions are summarized in Section 6.

2. Methods

In this section, the approach of simulating observation for ground tracking stations and the combined GNSS/LEO DD observation equations is introduced in details, respectively. Especially, considering the need to parameterize the atmospheric delays for medium and long baselines, the observation models have been of short, medium-to-long baseline types.

2.1. Data Simulation

In this study, we simulate the LEO and GNSS observations for ground tracking stations. And a new system is designed by introducing the LEO ranging satellites transmitting similar frequency signals on the L1 and L2 bands to the GPS. The data simulation is essentially the reverse process of positioning, so the receiver/satellite position and clock are all known values in observation simulation processing. On this basis, the satellite-to-receiver geometric range can be computed, and the various range errors are also calculated by observation models, all which are finally brought together to constitute simulating observations with the random noise [23]. Moreover, the atmospheric residuals cannot be ignored for medium-to-long baselines, the ionospheric and tropospheric delays are simulated strictly according to the existing models to make the simulation situation as close as possible to reality.

The observation equations for the undifferenced (UD) pseudorange P and carrier phase Φ, respectively, can be expressed as:

$$P^s_{r,f,i} = \rho^s_{r,i} - t_i{}^s + t_{r,i} + I^s_{r,f,i} + T^s_{r,i} + b^s_f + b_{r,f} + e^s_{r,f,i} \tag{1}$$

$$\Phi^s_{r,f,i} = \rho^s_{r,i} - t_i{}^s + t_{r,i} - I^s_{r,f,i} + T^s_{r,i} + \lambda_f N^s_{r,f} + B^s_f + B_{r,f} + \varepsilon^s_{r,f,i} \tag{2}$$

with the subscript f = 1, 2, and i = 1, ... , denote the carrier frequency and the epoch number, respectively; the superscript s and subscript r refer to the satellite and receiver respectively; $P^s_{r,f,i}$ and $\Phi^s_{r,f,i}$ are code and phase observations which need to be simulated at epoch i; $\rho^s_{r,i}$ is the geometric distance between the phase centers of satellite and receiver antennas;$t_i{}^s$ and $t_{r,i}$ are the satellite and receiver clock offsets; $I^s_{r,f,i}$ is the ionospheric delay at the frequency f; $T^s_{r,i}$ is the tropospheric delay; b^s_f and $b_{r,f}$ are the code hardware delays for satellite and receiver signal, respectively; λ_f is the wavelength of frequency f and $N^s_{r,f}$ is the integer ambiguity; B^s_f and $B_{r,f}$ are the satellite-dependent and receiver-dependent uncalibrated phase delay; $e^s_{r,f,i}$ and $\varepsilon^s_{r,f,i}$ denote the mixture of measurement noise and multipath error for code and phase observations, respectively.

In terms of pseudorange and phase observation simulation, the primary concern is to calculate all the components on the right side of (1) and (2). Meanwhile, considering the atmospheric residuals are the main cause of DD ambiguity resolution, the ionospheric and tropospheric delays will be simulated based on the real observables. The ionospheric delay is related to the total electron content (TEC) which can be calculated by the global ionosphere maps (GIM) from Center for Orbit Determination in Europe (CODE). Particularly, the ionospheric-delay simulation of the LEO observation must multiply by one related coefficient based on GIM calculations due to the large difference with GNSS satellites in orbit altitude [24]. Regarding the tropospheric delays, which consist of the dry and wet components, can be calculated by zenith delay and corresponding mapping function for the ground tracking stations. The wet delay adopts the estimated values from multi-GNSS PPP resolution, and the dry delay is computed by the Saastamonien model together with the Global Mapping Function (GMF) [25–27]. Besides, the DD observation models are sufficiently insensitive to the clock biases, as well as the code biases and the phase delay of satellite and receiver, which can be eliminated or weakened through between-station and between-satellite single differenced (SD) equations [10]. But these errors in simulating process are still taken into consideration to ensure the simulated data much closer to real data. The observation noises are simulated as a zero-mean normal distribution with the standard deviation (STD) dependent on satellite elevation angle, of which the STDs for each frequency are set to 20 cm and 2 mm for code and phase observation in the zenith direction, respectively [28].

2.2. Combined GNSS/LEO RTK Observation Model

The observation models for combined GNSS/LEO RTK in this study have been of the short, medium, and long single-baseline types. Hence, the processing methods of atmospheric delay must be taken into account when it comes to different-length baseline situations. This determines whether the ionospheric and tropospheric residuals are used as parameter estimations in the DD observation equations. After constructing between-station and between-satellite SD equations based on above-mentioned (1) and (2), the delays common to satellite and station part can be eliminated or ignored. Considering the existence of DD ionospheric and tropospheric delay, the DD pseudorange and carrier-phase observation equations can be described as:

$$\begin{cases} P^{G_1G_2}_{r_1r_2,f,i} = \rho^{G_1G_2}_{r_1r_2,i} + I^{G_1G_2}_{r_1r_2,f,i} + T^{G_1G_2}_{r_1r_2,i} + e^{G_1G_2}_{r_1r_2,f,i} \\ P^{L_1L_2}_{r_1r_2,f,i} = \rho^{L_1L_2}_{r_1r_2,i} + I^{L_1L_2}_{r_1r_2,f,i} + T^{L_1L_2}_{r_1r_2,i} + e^{L_1L_2}_{r_1r_2,f,i} \end{cases} \tag{3}$$

$$\begin{cases} \Phi^{G_1G_2}_{r_1r_2,f,i} = \rho^{G_1G_2}_{r_1r_2,i} - I^{G_1G_2}_{r_1r_2,f,i} + T^{G_1G_2}_{r_1r_2,i} + \lambda_{f,G} N^{G_1G_2}_{r_1r_2,f} + \varepsilon^{G_1G_2}_{r_1r_2,f,i} \\ \Phi^{L_1L_2}_{r_1r_2,f,i} = \rho^{L_1L_2}_{r_1r_2,i} - I^{L_1L_2}_{r_1r_2,f,i} + T^{L_1L_2}_{r_1r_2,i} + \lambda_{f,L} N^{L_1L_2}_{r_1r_2,f} + \varepsilon^{L_1L_2}_{r_1r_2,f,i} \end{cases} \tag{4}$$

With

$$\begin{cases} \rho^{s_1s_2}_{r_1r_2,i} = \left(\rho^{s_2}_{r_2,i} - \rho^{s_2}_{r_1,i}\right) - \left(\rho^{s_1}_{r_2,i} - \rho^{s_1}_{r_1,i}\right) \\ I^{s_1s_2}_{r_1r_2,f,i} = \left(I^{s_2}_{r_2,f,i} - I^{s_2}_{r_1,f,i}\right) - \left(I^{s_1}_{r_2,f,i} - I^{s_1}_{r_1,f,i}\right) \\ T^{s_1s_2}_{r_1r_2,i} = \left(T^{s_2}_{r_2,i} - T^{s_2}_{r_1,i}\right) - \left(T^{s_2}_{r_2,i} - T^{s_2}_{r_1,i}\right) \\ N^{s_1s_2}_{r_1r_2,f} = \left(N^{s_2}_{r_2,f} - N^{s_2}_{r_1,f}\right) - \left(N^{s_1}_{r_2,f} - N^{s_1}_{r_1,f}\right) \\ e^{s_1s_2}_{r_1r_2,f,i} = \left(e^{s_2}_{r_2,f,i} - e^{s_2}_{r_1,f,i}\right) - \left(e^{s_1}_{r_2,f,i} - e^{s_1}_{r_1,f,i}\right) \\ \varepsilon^{s_1s_2}_{r_1r_2,f,i} = \left(\varepsilon^{s_2}_{r_2,f,i} - \varepsilon^{s_2}_{r_1,f,i}\right) - \left(\varepsilon^{s_1}_{r_2,f,i} - \varepsilon^{s_1}_{r_1,f,i}\right) \end{cases} \tag{5}$$

where L and G refer to LEO and GNSS system, respectively. The reference station is denoted using subscript r_1, the rover station is denoted with a subscript r_2. The index G_1 and L_1 stand for reference satellites of each system, while the non-reference satellites are denoted using G_2 and L_2, respectively. The remaining symbols can refer to the meanings introduced in (1) and (2), but applicable for DD scheme here. Furthermore, it is worthy of indicating that all DD variables are expressed in meters, except the ambiguity which is expressed in cycles. And the label s is used to replace G and L for the sake of simply expression in (5).

Usually in the medium-to-long baselines, the relative slant ionospheric delays can be estimated as a parameter at each measurement epoch. For the tropospheric delay, the dry component is precisely corrected by a priori model, the wet component is estimated through setting up a zenith tropospheric delay (ZTD). Then, the linear observation equations of (3) and (4) can be expressed as:

$$\begin{cases} p^{G_1G_2}_{r_1r_2,f,i} = u^{G_1G_2}_{r_2,i} r_{r_1r_2,i} + \gamma_{f,G} \tilde{i}^{G_1G_2}_{r_1r_2,i} + m^{G_1G_2}_{r_2,i} \tau^{G_1G_2}_{r_1r_2,i} + \tilde{e}^{G_1G_2}_{r_1r_2,f,i} \\ p^{L_1L_2}_{r_1r_2,f,i} = u^{L_1L_2}_{r_2,i} r_{r_1r_2,i} + \gamma_{f,L} \tilde{i}^{L_1L_2}_{r_1r_2,i} + m^{L_1L_2}_{r_2,i} \tau^{L_1L_2}_{r_1r_2,i} + \tilde{e}^{L_1L_2}_{r_1r_2,f,i} \end{cases} \tag{6}$$

$$\begin{cases} \varphi^{G_1G_2}_{r_1r_2,f,i} = u^{G_1G_2}_{r_2,i} r_{r_1r_2,i} - \gamma_{f,G} \tilde{i}^{G_1G_2}_{r_1r_2,i} + m^{G_1G_2}_{r_2,i} \lambda^{G_1G_2}_{r_1r_2,i} + \lambda_{f,G} n^{G_1G_2}_{r_1r_2,f} + \tilde{\varepsilon}^{G_1G_2}_{r_1r_2,f,i} \\ \varphi^{G_1G_2}_{r_1r_2,f,i} = u^{G_1G_2}_{r_2,i} r_{r_1r_2,i} - \gamma_{f,G} \tilde{i}^{G_1G_2}_{r_1r_2,i} + m^{G_1G_2}_{r_2,i} \lambda^{G_1G_2}_{r_1r_2,i} + \lambda_{f,G} n^{G_1G_2}_{r_1r_2,f} + \tilde{\varepsilon}^{G_1G_2}_{r_1r_2,f,i} \end{cases} \tag{7}$$

where p and φ are the vectors of the observed-minus-computed code and phase observables, respectively; u is the corresponding design matrix that captures the relative receiver-satellite geometry; r is the 3-vector of incremental baseline coordinates; γ denotes the conversion factor of ionospheric delay from GNSS or LEO first frequency f_1 to current frequency f_j, $\gamma = f_1^2/f_j^2$; $\widetilde{i}$ is the DD ionospheric slant delay at f_1; m is the mapping function to get wet ZTD τ; n is the unknown integer DD ambiguities; $\widetilde{e}$ and $\widetilde{\varepsilon}$ denote the vectors of unmolded effects and measurement noise, respectively. So the unknown parameter vector for medium and long baselines is:

$$\mathrm{X} = [r^T, \tau, \widetilde{i}^T, n^T]^T \tag{8}$$

where T means transpose of the vector, and we omit subscripts and superscripts in the equation for brevity.

In terms of the short baseline, since the relative atmospheric delays can be assumed absent, the unknown parameter vector is:

$$\mathrm{X} = \left[r^T, n^T\right]^T \tag{9}$$

For the combined GNSS/LEO RTK model, the observations from all satellites are processed simultaneously in a single adjustment. All unknown parameters are obtained by extended Kalman filter (EKF) estimator, then the well-known LAMBDA method is employed to solve the DD ambiguity-fixed problem [29]. After the validation by the simple ratio-test, the fixed solution of the non-ambiguity parameter vectors including the rover positions are obtained based on fixed ambiguity parameters. In addition, the detailed data processing strategy is presented in the subsequent section.

3. Situation and Strategy

In this section, we will introduce the constellation configuration, simulation situation, and data processing strategy, respectively. Firstly, four kinds of LEO constellations with different satellite numbers, as well as nominal GPS constellation with full operational capability, are adopted in order to investigate different LEO constellations augmented performances. Then, the station distribution and its support constellation are described, together with length information of different baselines. Finally, in terms of the short and medium-to-long baselines, different data processing strategies of RTK solutions are set to make a preparation for the assessment of combined GPS/LEO RTK for different length baselines in detail.

3.1. Constellation Configuration

In this work, four kinds of LEO constellations are simulated through Satellite Tool Kit (STK) [30] software to study the influence of LEO satellite number on augmented GNSS RTK performance, where 60-, 96-, 192-, and 288-LEO satellites schemes are selected for analysis, respectively. Aim for achieving the global coverage, these LEO satellites are allocated to 10 or 12 equally spaced orbital planes, with 6~24 satellites in each plane. Furthermore, these orbital planes of different LEO constellations, all belong to the polar circular orbits, are inclined at 90° to the equatorial plane and 1000 km in altitude [23]. And the detailed information of four LEO constellations is given in Table 1. Besides, the 24 GPS simulated satellites based on the nominal constellation configurations, are equally distributed over medium earth orbits and assigned in six orbital planes with a 56° inclination angle at 20,180 km in altitude [31]. Slots for the GPS 24-slot constellation are specified in terms of the Right Ascension of the Ascending Node (RAAN) and the Argument of Latitude, all which are listed in Table 2.

Figure 1 shows the simulated constellations of GPS and LEO satellites, all of which clearly display the scale difference above the earth. As can be observed, the LEO satellites are very close to the earth, which means that the LEO satellites can move faster than GPS satellites during the same period. Compared with the 3.87 km/s operational speed and 11.97 h orbital period of GPS satellite, the LEO satellite at 1000 km orbit can reach speeds of 7.35 km/s and the correspondingly orbital period is about 1.75 h. However, at meanwhile, the above-mentioned phenomena also imply that the LEO constellation with smaller footprint must require more satellites to achieve global coverage. It is acknowledged that the 288-LEO scheme exhibits the best coverage of satellite visibility on a global scale. Based on this, more numbers of LEO satellites transmitting GNSS-like signals will help to improve observation quality and utilization for the ground tracking stations.

Table 1. Detailed orbital configurations of low earth orbit (LEO) constellations.

Orbit	LEO	LEO	LEO	LEO
Satellite Number	60	96	192	288
Altitude[km]	1000	1000	1000	1000
Constellation	10 planes × 6 satellites	12 planes × 8 satellites	12 planes× 16 satellites	12 planes× 24 satellites
Inclination[deg]	90	90	90	90

Table 2. Slot assignments of the nominal GPS constellation. RAAN: Right Ascension of the Ascending Node.

Slot	RAAN	Argument of Latitude	Slot	RAAN	Argument of Latitude
A1	272.847°	268.126°	D1	92.847°	135.226°
A2	272.847°	161.786°	D2	92.847°	265.446°
A3	272.847°	11.676°	D3	92.847°	35.156°
A4	272.847°	41.806°	D4	92.847°	167.356°
B1	332.847°	80.956°	E1	152.847°	197.046°
B2	332.847°	173.336°	E2	152.847°	302.596°
B3	332.847°	309.976°	E3	152.847°	66.066°
B4	332.847°	204.376°	E4	152.847°	333.686°
C1	32.847°	111.876°	F1	212.847°	238.886°
C2	32.847°	11.796°	F2	212.847°	345.226°
C3	32.847°	339.666°	F3	212.847°	105.206°
C4	32.847°	241.556°	F4	212.847°	135.346°

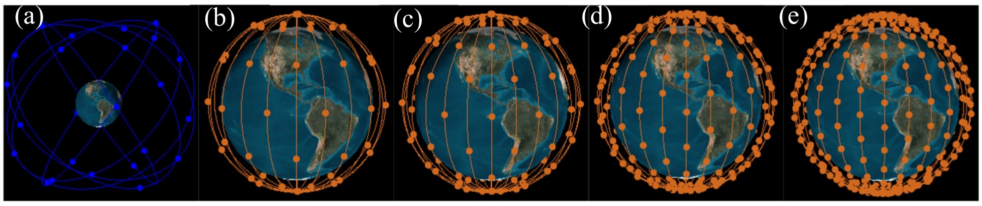

Figure 1. GPS and LEO constellations. (**a**) GPS; (**b**) 60 LEO; (**c**) 96 LEO; (**d**) 192 LEO; (**e**) 288 LEO.

3.2. Simulation Situation

In order to investigate the performances of LEO constellation augmented GNSS RTK positioning with different length, we selected 19 Continuously Operating Reference Stations (CORS) run by U.S. National Geodetic Survey (NGS) at the mid-latitudes, which can provide the fixed station coordinates and support to track the real GPS constellation for ground-based observation simulation. The corresponding locations of the simulated stations are shown in Figure 2, mainly in 30–48°N region. As can be observed, these mid-latitude CORS stations distributed at different distances constitute short, medium and long baselines. The small scale map presents the area where the five stations make up short baselines, while the larger one covering a wider area and more stations provides the possibility of forming medium-to-long baselines. And the specific lengths of all baselines are also given in Table 3. Furthermore, considering that the low operating altitude of LEO satellites can cause the fast motion with respect to the ground stations in a relatively short period, the sampling interval of simulating observations is set 1 s in order to best analyze the effect of LEO satellites for GPS RTK positioning.

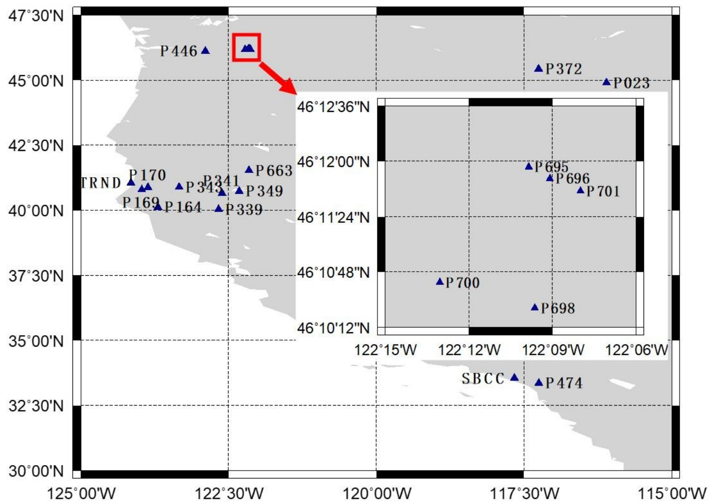

Figure 2. Distribution of stations at the mid latitudes. The small map shows the stations constituting short baselines and the larger one is for medium-to-long baselines.

Table 3. Length information of the short, medium and long baselines at mid latitudes.

Short Baselines		Medium Baselines		Long Baselines	
P696-P695	1.1 km	P169-TRND	33.0 km	P170-P339	138.2 km
P698-P696	2.8 km	SBCC-P474	44.2 km	P698-P372	390.5 km
P700-P695	4.7 km	P446-P698	57.0 km	P698-P663	514.7 km
P700-P696	5.5 km	P339-P341	68.7 km	P698-P349	604.7 km
P700-P701	6.8 km	P164-P339	88.0 km	P023-P343	739.2 km

3.3. Data Processing Strategy

According to the Table 4, the estimated parameters, observation models and index settings of DD observables are showed to describe the data processing strategy for LEO augmented GNSS RTK in details. Then, based on above-mentioned simulated GPS and LEO observations, we can comprehensively analyze the RTK performances of different constellation schemes including the GPS-only scheme, as well as the combined constellation schemes of GPS with 60, 96, 192, and 288 LEO satellites, respectively. Especially for the different length baselines, the appropriate processing strategy must be adopted for the atmospheric residuals, otherwise it will hinder successful ambiguity resolution. Meanwhile, this study will only consider observation models of the single-baseline type, using two stationary receivers separated by different distances. This means that the ionospheric and tropospheric delay can be significantly reduced by forming DD observation equations for the short-range RTK solutions, but not for that of medium- and long-range baselines. However, the DD ionospheric and tropospheric delay can be set to zero initially and estimate them as a random walk in each processing session for medium-to-long baselines. Especially for the subsequent epoch, the atmospheric parameters and variances can employ the estimated results of last epoch as prior estimation values, where the atmospheric variances usually need to add a process noise. As for the vertical ionospheric delay, its process noise is set as $10^{-3}m/\sqrt{s}$. So the empirical model can be expressed as follow:

$$\left\{ \begin{array}{c} \sigma_{ion}^2 = k\, q_{ion}^2\, \Delta t \\ q_{ion} = 10^{-3}\left(bl/10^4 \cos(el)\right) m/\sqrt{s} \end{array} \right. \tag{10}$$

where σ_{ion} is the ionospheric process noise; q_{ion} denotes the spectrum densities of random process for ionospheric parameter; bl is the length of baseline; el is the satellite elevation angle; Δt is the sampling interval; k is the coefficient to distinguish GPS and LEO satellite, which is set 1 for GPS satellite. Considering the fact that the different motion speed of GPS and LEO satellite leads to a ionospheric variation between adjacent epochs, the ionospheric process noise need to be adjusted for LEO-satellite observation. For the 30 s low sampling-interval data, the slant ionospheric delay varies a lot due to the fast motion of LEO satellite, thus the ionospheric process noise should be enlarged compared to that for GPS satellite. But for the high sampling-interval data, i.e., 1 s observation, it is usually insensitive to ionospheric variation. So in this study, the coefficient k for LEO satellite is also set 1 for the data with sampling interval. Meanwhile, it is noted that some cycle slip detection algorithms also need to be adjusted for LEO-satellite observation based on the above-mentioned consideration, such as the geometry-free combination method. The cycle-detection threshold can adopt a similar adjustment principle to that for the ionospheric process noise. For the tropospheric process noise, it is calculated by the process noise of wet ZTD and the sampling interval in this study, the empirical model can be expressed as follow:

$$\sigma_{trop}^2 = q_{trop}^2 \, \Delta t \tag{11}$$

where σ_{trop} is the ionospheric process noise; q_{trop} is the process noise of wet ZTD, which is set as $10^{-4}\ m/\sqrt{s}$. In addition, the code and phase error ratio of each frequency can be set based on an empirical value, e.g., 100:1. The observation weight is also used according to the criterion of elevation-dependent weight. Noteworthily, the large LEO constellation brings the challenge of high-dimensional ambiguity resolution. Once all ambiguities are simultaneously failed to fix, partial ambiguity-fixed strategy can be adopted to resolve a subset of the candidate ambiguities during data processing [32].

Table 4. Data processing strategy for LEO augmented GPS RTK (real-time kinematic).

Items	Models
Satellites	GPS (G); GPS+LEO (GL);
Estimator	Extended Kalman filter (EKF)
Observations	Pseudorange and carrier phase observations
Signal selection	GPS: L1/L2; LEO: L1/L2
Sampling Interval	1s
Elevation mask	7.5°
Observation weight	Elevation dependent weight
Satellite orbit	Precise ephemeris by STK
Satellite clock	DD elimination or weakening
Receiver clock	DD elimination or weakening
Station coordinate	Estimated in kinematic mode
Ionospheric delay	Short baselines: Not estimated; Medium-to-long baselines: Estimated
Tropospheric delay	Short baselines: Not estimated; Medium-to-long baselines: Estimated
Process noise of vertical iono.delay	10^{-3} m/sqrt(s)
Process noise of wet ZTD	10^{-4} m/sqrt(s)
Phase ambiguity	LAMBDA
Ratio	3.0
Code/carrier-phase error ratio	100

4. Performance of Different LEO Constellations Augmented GPS RTK

To get a representative evaluation of LEO constellations augmented GPS RTK with different numbers of LEO satellites, the 'P339-P341′ baseline scheme is taken as an example to analyze the augmentation performance based on the simulated polar-orbiting data of 60, 96, 192, and 288 LEO satellites. The simulation data for ground stations covered 2 h from 12:30 to 14:30 on January 1, 2017, and which has been initialized to recalculate every half an hour in RTK positioning processing. Thus there are four computations for one baseline in 2-h observations to ensure the reliability of positioning results by using the statistical averages, including the average convergence time, time to first fix (TTFF), fixing ratio, visible satellite number, position dilution of precision (PDOP) value, and baseline solution precision. In this context, the convergence time is defined as the time required to keep horizontal errors reaching and afterward remaining within 0.1 m. The fixing ratio reflects the ambiguity-fixed situation after the validation by the ratio-test with the critical value of 3, which can be defined as the ratio of the numbers of ambiguity-fixed epochs to the numbers of all epochs. The baseline solution precision is an indicator to directly judge coordinates accuracy in RTK solution, which can be expressed by the root mean square (RMS) errors after successfully fixing ambiguity in east, north and up baseline components. Moreover, the reference values of baseline components can be calculated in view of known station coordinates provided by NGS.

Figure 3 presents the GPS RTK results with the augmentations of different LEO satellite numbers for 'P339-P341′ baseline scheme. According to Figure 3a–c and the local enlarged Figure 4, the introduction of LEO satellites does contribute for accelerating the convergence of GPS RTK, no matter in the east, north and up components. And observing more LEO satellites yields shorter convergence time. And we can also see that the precision of the vertical component is obviously worse than that of horizontal components. Figure 3d, e show the corresponding numbers of visible satellites and the PDOP values of different constellation schemes, respectively. Depending on the location of ground tracking station, the average number of tracked GPS-only satellites is 7.13 and the PDOP value is 1.97. When combining with 60-, 96-, 192-, and 288-LEO constellations, the visible satellite numbers can correspondingly increase by 1.1, 3.4, 6.8, and 9.5, respectively. Meanwhile, the average PDOP values can also decrease to 1.76, 1.57, 1.31, and 1.1, respectively. Besides, the fast movement of the LEO satellite can be observed from the rapid variation of PDOP values.

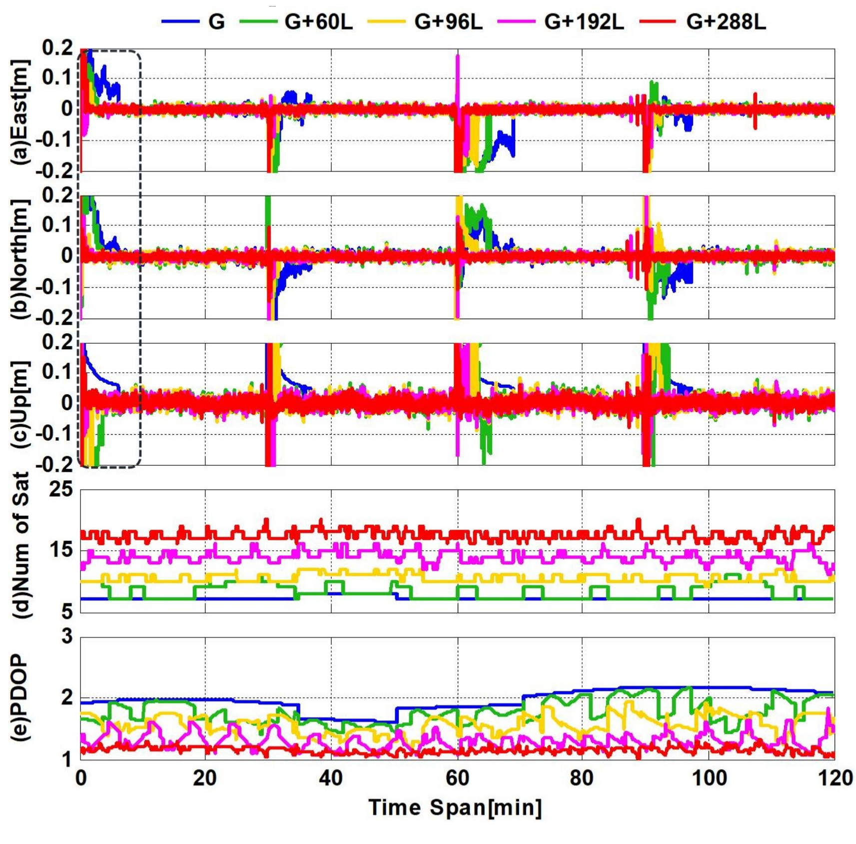

Figure 3. Comparisons of different scales of LEO constellations augmented GPS RTK solutions in east, north, and up components, respectively, for 'P339-P341′ baseline scheme. The visible satellite numbers and position dilution of precision (PDOP) values are also presented.

In order to analyze the baseline solution precision after fixing ambiguity, the mean RMS errors in the east, north, and up baseline components for different LEO constellation schemes are given in Table 5. For the GPS-only scheme, the baseline solution precision is 0.77, 0.93, and 1.73 cm in east, north, and up baseline components, respectively. By introducing the different scales of LEO constellations, the RMS errors can be best reduced to 0.58, 0.65, and 1.37 cm, respectively. Obviously, whether or not to introduce LEO satellites, the RTK positioning precisions can all attain millimeter level in horizontal directions and centimeter level in the elevation direction after fixing DD ambiguities. Nevertheless, the larger LEO constellation is conducive to achieve more stable and better positioning accuracy. Such as 288-LEO constellation scheme, the solution precisions of east, north, and up baseline components can be increased by 25, 30, and 21%, respectively.

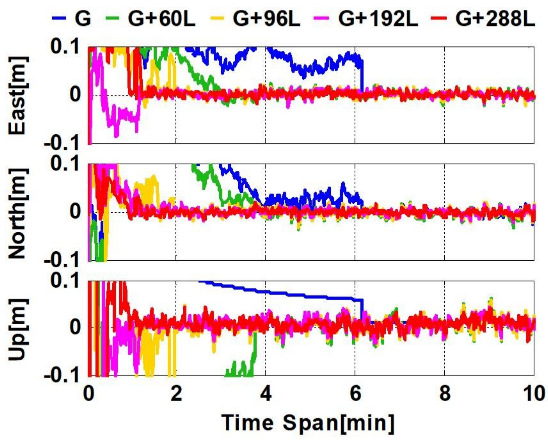

Figure 4. The local enlarged picture of the Figure 3 (dotted box) shows the first 10-min comparison of different scales of LEO constellations augmented GPS RTK solutions at three components, for 'P339-P341′ baseline scheme.

Table 5. Statistics of the baseline solution precisions after fixing ambiguity in three directions.

RMS[cm]	GPS-Only	G+60L	G+96L	G+192	G+288L
East	0.77	0.76	0.71	0.62	0.58
North	0.93	0.90	0.83	0.69	0.65
Up	1.73	1.71	1.67	1.55	1.37

Figure 5 shows the average convergence time, TTFF and fixing ratio for different LEO constellations augmented GPS RTK solutions, respectively. We can find that the augmented performances are closely related to the numbers of LEO satellites. Along with the increasing LEO satellites, the average convergence time and TTFF of RTK positioning will be much shorter, as well as higher fixing ratio. Compared with the GPS-only scheme, the convergence time can be reduced from 4.94 to 2.73, 1.47, 0.92, and 0.73 min by combination with observations from 60, 96, 192, and 288 LEO satellites, respectively. And the TTFF can be shortened from 7.28 to 3.33, 2.38, 1.22, and 0.87 min, respectively. Furthermore, the corresponding fixing ratio can be increased by 11.85, 16.33, 19.38, and 20.16%, respectively. Especially for 192- or 288-LEO constellation scheme, the improvements on RTK convergence and fixing speeds are more significant contrast to that of GPS-only, the convergence time can be shortened from about 5 min to within 1 min, where the TTFF is also realized from about 7 to about 1 min. Meanwhile, both schemes can reach above 95% average fixing ratio.

Figure 6 shows 1-h sky plots (azimuth (0–360°) versus elevation (0–90°)) of GPS with the augmentation of 60, 96, 192, and 288 polar-orbiting LEO satellites, respectively. As can be observed, the circular markers illustrate the positions of visible satellites at the initial epoch. Compared with the GPS-only scheme, the number of visible satellites is gradually increasing with the introduction of LEO satellites. At meanwhile, the LEO constellations consisting of 96, 162, and 288 satellites, as augmentations or complements to GPS satellites, can nearly fill the coverage gap above rover station, except that of 60 satellites. Moreover, noting that the GPS elevation mostly varies from 0° to 30° over an hour, while LEO satellites can streak much longer tracks with the elevation variations from 0° to

90° during the same period, which contributes for improving GPS RTK positioning as a result of the rapid geometric change.

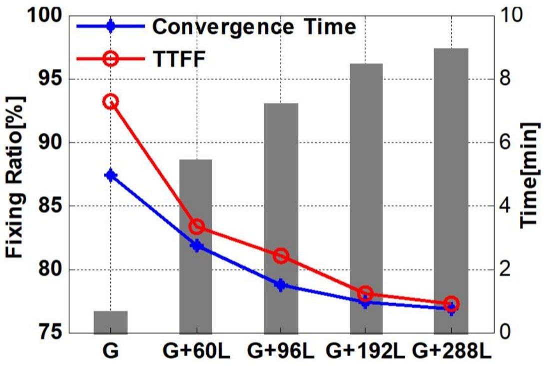

Figure 5. Average convergence time, time to first fix (TTFF), and fixing ratio of GPS RTK solutions in combination with different LEO constellations, for 'P339-P341′ baseline scheme.

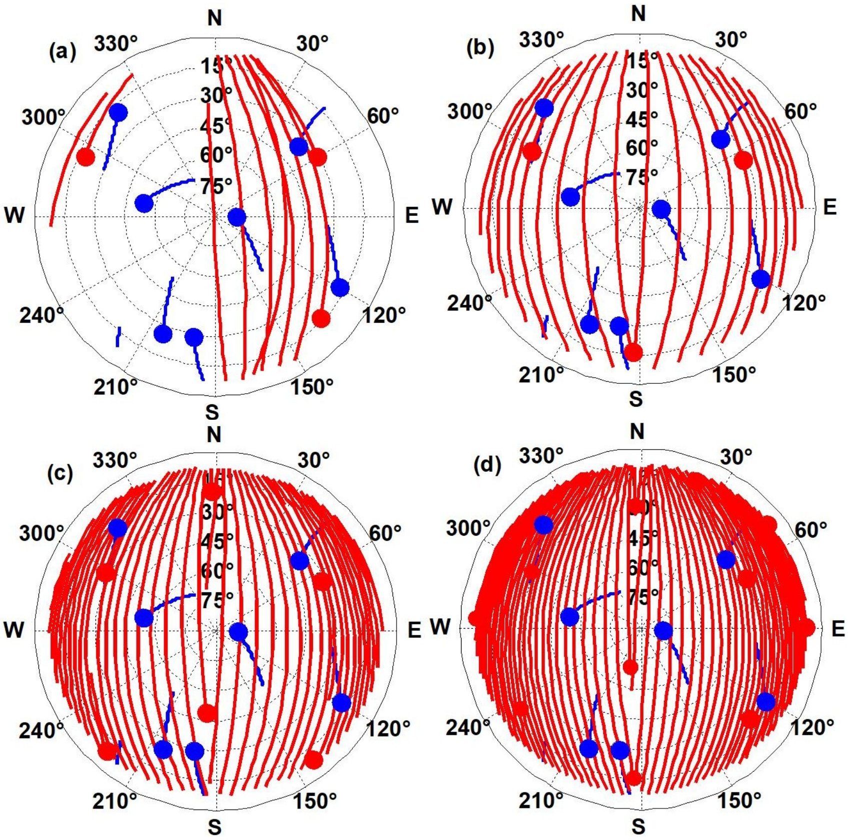

Figure 6. The 1-h sky plots (azimuth versus elevation) of GPS with the augmentations of different LEO constellations: (**a**) GPS+60 LEO; (**b**) GPS+96 LEO; (**c**) GPS+192 LEO; (**d**) GPS+288 LEO. Circular markers indicate the satellite (GPS in blue, LEO in red) positions at the initial epoch.

5. Assessment of Combined GPS/LEO RTK for Different Length Baselines

With the aforementioned characteristics of the LEO constellation augmented GPS RTK positioning, the RTK computations for 15 different length baselines, see Table 3, are conducted in this section, just like 'P339-P341′ baseline scheme. Afterward, we made simple statistics on the average convergence time and TTFF for each baseline type, and analyze the influences of LEO constellations on short-, medium-, and long-baseline solutions, respectively. Furthermore, it is noteworthy that the distinguishing atmospheric processing strategies must be taken into account for achieving better positioning performance under different circumstance.

5.1. RTK for Short Baselines

In this statistic analysis, 5 representative short baselines with lengths less than 10 km are chosen to evaluate the RTK performance with the augmentation of different numbers of LEO satellites, where the atmospheric residuals can be assumed absent through DD equations. Figure 7 shows the average convergence time and TTFF of different LEO constellations augmented GPS RTK solutions. It can be clearly found that the RTK solutions for short baseline schemes can easily converge or fix within a few seconds, whether or not LEO satellites are introduced. As the baseline range becomes much shorter, the augmented effectiveness gradually becomes unobvious for the LEO satellite numbers. After further statistics of average convergence time and TTFF of all short-baseline solutions, the 60- and 96-LEO schemes can achieve convergence and fixing in about 2 s, compared with that of about 4 s for the GPS-only scheme. And the slightly better augmentation performances can be realized within about 1 s for 192- and 288-LEO schemes.

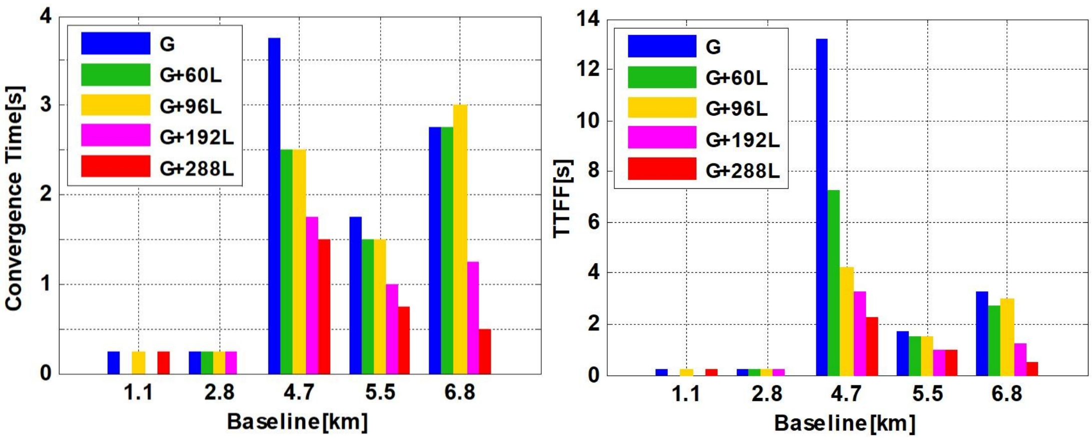

Figure 7. Average convergence time (**left panel**) and TTFF (**right panel**) of different LEO constellations augmented GPS RTK positioning for five short baselines.

5.2. RTK for Medium-to-Long Baselines

In order to better investigate the augmentation performances of different LEO constellations for medium- and long-baseline RTK positioning, the medium baselines of 33.0, 44.2, 57.0, 68.7, and 88.0 km, as well as the long baselines of 138.2, 390.5, 514.7, 604.7, and 739.2 km, are selected for analysis from the perspectives of convergence time and TTFF. Meanwhile, it is noted that the DD ionospheric and tropospheric delays need to be considered as estimated parameters in medium-to-long baseline schemes.

Figure 8 presents the average convergence time and TTFF of different-baseline schemes with the augmentations of different LEO constellations. It is obvious to see that the convergence time and TTFF are gradually getting longer with the increase of baseline length. For one specific baseline, the LEO constellation can make a significant contribution to the convergence and ambiguity-fixed performances. Especially for the 192- and 288-satellite constellations, the average convergence time and TTFF for all baselines can be shortened by about more than 80% and even reach to about 1 min. At meanwhile, it also can be found that the long-range improvement is a little better than medium-range one.

Further statistics about LEO constellation-augmentation performances in above-mentioned medium- and long-baseline schemes are demonstrated in Figure 9. Through introducing LEO constellations consisting of 60, 96, 192, and 288 satellites, the correspondingly average convergence time for medium baselines can be shortened from 4.19 to 2.7, 1.54, 0.77, and 0.48 min, and that for long baseline are dramatically decreased from 8.55 to 4.56, 2.55, 0.96, and 0.80 min, compared with the

GPS-only scheme. As for the average TTFF, the statistical time for medium baselines can be shortened from 7.11 to 4.03, 2.56, 1.22, and 0.90 min, respectively. More obvious improvement is observed for the long baselines, which can reduce the TTFF from 12.34 to 7.44, 3.62, 1.62, and 1.31 min, respectively. As a result, the convergence and ambiguity-fixed speeds of RTK positioning can indeed be significantly improved with the addition of LEO satellites. The larger LEO constellations, the better improvement.

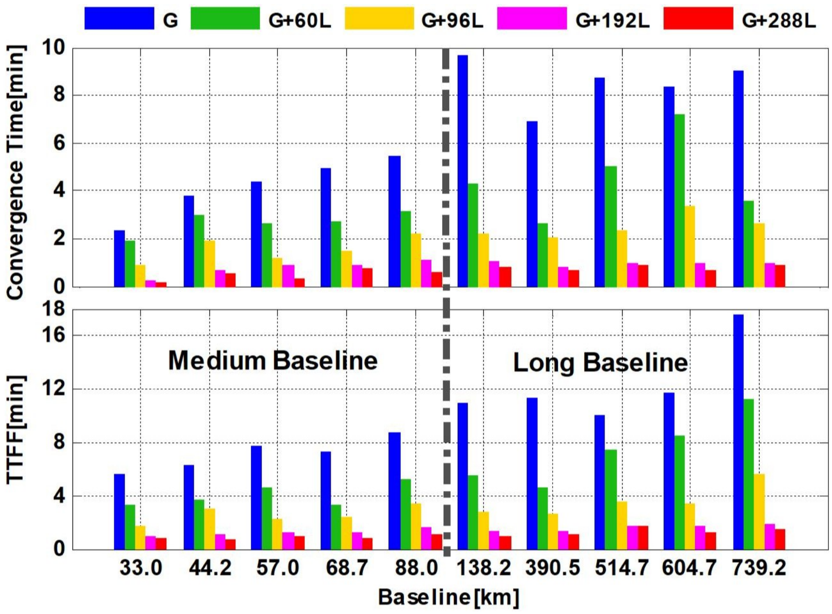

Figure 8. Average convergence time and TTFF of different LEO constellations augmented GPS RTK positioning for ten medium-to-long baselines.

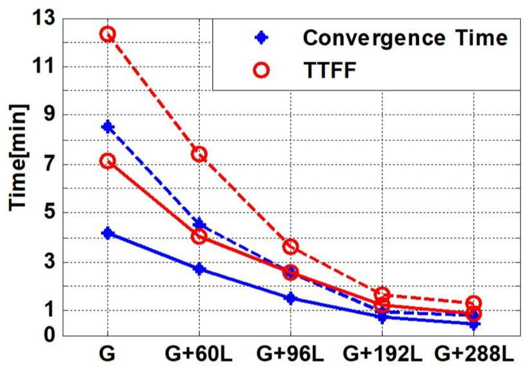

Figure 9. The solid lines describe the average convergence time and TTFF of five medium-baseline solutions with the augmentations of different LEO constellations, and the similar indexes of five long-baseline solutions are shown in dashed line.

6. Conclusions

Aiming at investigating the performance of LEO constellations augmented GNSS RTK positioning, four kinds of LEO constellations with different satellite numbers and the nominal GPS constellation were adopted for analysis in this study. Based on the simulated GPS+LEO pseudorange and carrier-phase observations at the ground tracking stations, the augmentation performances of the single-baseline RTK solutions were comprehensively evaluated from the aspects of average convergence time, TTFF, fixing ratio, visible satellite number, PDOP value, and baseline solution precision.

As for the different scales of LEO constellations augmented GPS RTK solutions, it was found that the improvement performances are closely related to the number of LEO satellites. The more LEO satellites are available, the less convergence time and TTFF can be achieved in RTK positioning, as well as the higher fixing ratio. The corresponding statistical results from a 68.7-km scheme show that when introducing 60-, 96-, 192-, and 288-LEO constellations, the convergence time can be shortened from 4.94 to 2.73, 1.47, 0.92, and 0.73 min, respectively. Furthermore, the TTFF can be decreased to 3.33, 2.38, 1.22, and 0.87 min, respectively, compared with that of 7.28 min for GPS-only scheme. Meanwhile, the fixing ratio can be also increased by 11.85, 16.33, 19.38, and 20.16%, respectively. Particularly, for 192- and 288-satellite LEO constellations, the improvement on RTK convergence and fixing is more obvious in contrast to that of the GPS-only scheme, where the convergence time and TTFF can be shortened to about 1 min and the average fixing ratio can reach above 95%. Owing to that more visible LEO satellites can move faster and streak longer tracks than GPS satellites during the same period, which contributes to the better geometric diversity at stations. Furthermore, the baseline solution precision is further analyzed to see whether or not similar RTK positioning precision can be obtained with the augmentations of different scales of LEO constellations after fixing DD ambiguities. It is found that adopting larger LEO constellations are conducive to achieve more stable and better positioning accuracy.

Considering that the improved performance may be associated with different length baselines, 15 sample baselines in mid-latitude regions were selected for analysis. For short-baseline schemes, the average convergence time and TTFF can easily reach to within a few seconds, whether or not to introduce LEO satellites. For the medium and long baseline schemes, the statistical results of all baselines confirm that more LEO satellites can achieve faster convergence and fixing, but we have also noticed that it is still difficult to achieve instantaneous ambiguity-fixing. Besides, the improvement of long-baseline scheme is more obvious than that of the medium-baseline scheme, and the average TTFF for the long baselines can be shortened by about 90% from about 12 to within 2 min while introducing the larger LEO constellation of 192 or 288 satellites. As similar improvement can be observed from the convergence time.

Overall, we made an initial assessment of GNSS RTK positioning augmented with LEO satellites and proved that the LEO satellites can helpfully improve convergence and ambiguity-fixed performance, which provides an important insight into the DD ambiguity resolution for the medium- and long-range RTK solutions. In future researches, further studies are therefore necessary to evaluate the LEO constellation-augmentation performance for multi-baseline RTK and PPP-RTK solutions. The configuration optimization and constellation design of LEO satellites remain to be explored. Besides, there are some limitations in current observation simulation. For example, the simulation and processing of atmospheric residuals do not take into account the effects of high-order errors, and the ionospheric delay simulated on GIM calculations may cause distortions. Moreover, the actual built LEO navigation augmentation system in future may also has many unknown errors like inter-frequency and inter-system biases, causing problems of whether the existing error-source models are suitable for LEO-satellite scheme and of how to improve the current multi-constellation fusion algorithm, which should be carefully considered in real data processing. With the continuous development of LEO satellites, more attentions should be paid to the new problems and challenges when achieving LEO-augmented positioning in practical use. Though more available observations contribute to better positioning performance, they also bring a higher requirement for hardware equipment to possess more computing power and speed in data processing. Meanwhile, the algorithm of the high-dimensional ambiguity resolution will also face challenges and need to be further optimized. Considering the appearance of larger and diversified constellation, the ground receiver must be capable of supporting so many signal channels, and the corresponding ability to receive and storage data also needs to be improved. In addition, the problem of multi-signal interference may happen due to the harmonic distortion or insufficient band-pass filtering. Once these negative side effects haven been solved or eliminated, higher precision and better performance from LEO-satellite augmentation positioning can be expected.

Author Contributions: All authors contributed to the writing of this manuscript. X.L., H.L. and F.M. conceived and designed the experiments. H.L., F.M., J.L., and Z.J. processed the data, drew the pictures and investigated the results. X.L. and X.L. validated the data.

Funding: This study is financially supported by the National Natural Science Foundation of China (Grant No. 41774030), the Hubei Province Natural Science Foundation of China (Grant No. 2018CFA081) and the National Youth Thousand Talents Program.

Acknowledgments: We are very grateful to the reviewers for their helpful remarks for improving the manuscript. Meanwhile, we would also like to express our gratitude to NGS, IGS, MGEX, GFZ, DLR, and CODE for providing multi-GNSS data and products, as well as the help from Mohamed Freeshah and Renpan Wu. In addition, the numerical calculations in this study have been done on the supercomputing system in the Supercomputing Center of Wuhan University.

Conflicts of Interest: The authors declare no conflict of interest.

References

1. Odijk, D.; Wanninger, L. Differential Positioning. In *Springer Handbook of Global Navigation Satellite Systems*, 1st ed.; Teunissen, P.J.G., Montenbruck, O., Eds.; Springer International Publishing: Cham, Switzerland, 2017; pp. 763–773.
2. Odijk, D.; Verhagen, S.; Teunissen, P.J.G. Medium-Distance GPS Ambiguity Resolution with Controlled Failure Rate. In *Geodesy for Planet Earth*; Kenyon, S., Pacino, M., Marti, U., Eds.; Springer: Berlin/Heidelberg, Germany, 2012; Volume 136, pp. 745–751.
3. Tiberius, C.C.J.M.; Pany, T.; Eissfeller, B.; de Jong, K.; Joosten, P.; Verhagen, S. Integral GPS-Galileo Ambiguity Resolution. In Proceedings of the ENC GNSS 2002, Copenhagen, Denmark, 27–30 May 2002.
4. Takasu, T.; Yasuda, A. Kalman-Filter-Based Integer Ambiguity Resolution Strategy for Long-Baseline RTK with Ionosphere and Troposphere Estimation. In Proceedings of the 23rd International Technical Meeting of the Satellite Division of the Institute of Navigation, Portland, OR, USA, 21–24 September 2010; Volume 7672, pp. 161–171.
5. Teunissen, P.J.G. A new Method for Fast Carrier Phase Ambiguity Estimation. In Proceedings of the IEEE Position Location and Navigation Symposium, Las Vegas, NV, USA, 11–15 April 1994; pp. 562–573.
6. Teunissen, P.J.G. The Ionosphere-weighted GPS baseline precision in canonical form. *J. Geod.* **1998**, *72*, 107–111. [CrossRef]
7. Dai, L. Dual-frequency GPS/GLONASS Real-Time Ambiguity Resolution for Medium-Range Kinematic Positioning. In Proceedings of the 13th International Technical Meeting of the Satellite Division of the U.S. Institute of Navigation, Salt Lake City, UT, USA, 19–22 September 2000; pp. 1071–1080.
8. Odijk, D. Fast Precise GPS Positioning in the Presence of Ionospheric Delays. Ph.D. Dissertation, Faculty of Civil Engeenering and Geoscience, Delft University of Technology, Delft, the Netherlands, 2002.
9. Li, B.; Verhagen, S.; Teunissen, PJ.G. Robustness of GNSS integer ambiguity resolution in the presence of atmospheric biases. *GPS Solut.* **2014**, *18*, 283–296. [CrossRef]
10. Odolinski, R.; Teunissen, P.J.G.; Odijk, D. Combined GPS + BDS for short to long baseline RTK positioning. *Meas. Sci. Technol.* **2015**, *26*, 045801. [CrossRef]
11. Gomi, Y.; Tominaga, T.; Kubo, N.; Yasuda, A. B-2–38 The Ionospheric Effect on Medium Scale Network RTK. In Proceedings of the Institute of Electronics, Information and Communication Engineers (IEICE) General Conference, Tokyo, Japan, 8 March 2006; p. 276.
12. Pirti, A.; Gumus, K.; Erkaya, H.; Hosbas, R. Evaluating repeatability of RTK GPS/GLONASS near/under forest environment. *Croatian J. For. Eng.* **2010**, *31*, 23–33.
13. Yao, J.; Balaei, A.; Hassan, M.; Alam, N.; Dempster, A. Improving cooperative positioning for vehicular networks. *IEEE Trans. Veh. Technol.* **2011**, *60*, 2810–2823. [CrossRef]
14. Rabinowitz, M.; Spilker, J.J. A new positioning system using television synchronization signals. *IEEE Trans. Broadcast.* **2005**, *51*, 51–61. [CrossRef]
15. Enge, P.; Ferrell, B.; Bennet, J.; Whelan, D.; Gutt, G.; Lawrence, D. Orbital Diversity for Satellite Navigation. In Proceedings of the 25th International Technical Meeting of the Satellite Division of the Institute of Navigation (ION GNSS 2012), Nashville, TN, USA, 17–21 September 2012; pp. 3834–3846.
16. Enge, P.K.; Talbot, N.C.; San, J. Method and Receiver Using a Low Earth Orbiting Satellite Signal to Augment the Global Positioning System. U.S. Patent No. 5,812,961, 22 September 1998.

17. Rabinowitz, M.; Parkinson, B.W.; Cohen, C.E.; O'Connor, M.L.; Lawrence, D.G. A System using LEO Telecommunication Satellites for Rapid Acquisition of Integer Cycle Ambiguities. In Proceedings of the ION/IEEE Position Location and Navigation Symposium, Palm Springs, CA, USA, 20–23 April 1998; pp. 137–145.
18. Joerger, M.; Neale, J.; Pervan, B. Iridium/GPS Carrier Phase Positioning and Fault Detection over Wide Areas. In Proceedings of the 22nd International Technical Meeting of the Satellite Division of the Institute of Navigation (ION GNSS 2009), Savannah, GA, USA, 22–25 September 2009; pp. 1371–1385.
19. Joerger, M.; Gratton, L.; Pervan, B.; Cohen, C.E. Analysis of iridium-augmented GPS for floating carrier phase positioning. *Navigation* **2010**, *57*, 137–160. [CrossRef]
20. Tian, S.; Dai, W.; Liu, R.; Chang, J.; Li, G. System using-hybrid LEO-GPS satellites for rapid resolution of integer cycle ambiguities. *IEEE Trans. Aerosp. Electron. Syst.* **2014**, *50*, 1774–1785. [CrossRef]
21. Ke, M.; Lv, J.; Chang, J.; Dai, W.; Tong, K.; Zhu, M. Integrating GPS and LEO to Accelerate Convergence Time of Precise Point Positioning. In Proceeding of the IEEE 7th International Conference on Wireless Communications and Signal, Nanjing, China, 15–17 October 2015; pp. 1–5.
22. Ge, H.; Li, B.; Ge, M.; Zang, N.; Nie, L.; Shen, Y.; Schuh, H. Initial Assessment of Precise Point Positioning with LEO Enhanced Global Navigation Satellite Systems (LeGNSS). *Remote Sens.* **2018**, *10*, 984. [CrossRef]
23. Li, X.; Ma, F.; Li, X.; Lv, H.; Bian, L.; Jiang, Z.; Zhang, X. LEO constellation augmented multi-GNSS for rapid PPP convergence. *J. Geod.* **2018**. [CrossRef]
24. Yizengaw, E.; Moldwin, M.B.; Galvan, D.; Iijima, B.A.; Komjathy, A.; Mannucci, A.J. Global plasmaspheric TEC and its relative contribution to GPS TEC. *J. Atmos. Sol. Terr. Phys.* **2008**, *70*, 1541–1548. [CrossRef]
25. Saastamoinen, J. Atmospheric correction for the troposphere and stratosphere in radio ranging of satellites. In *The Use of Artificial Satellites for Geodesy*; AGU: Washington, DC, USA, 1972; Volume 15, pp. 247–251.
26. Boehm, J.; Niell, A.; Tregoning, P.; Schuh, H. Global mapping function (GMF): A new empirical mapping function based on numerical weather model data. *Geophys. Res. Lett.* **2006**, *33*, L07304. [CrossRef]
27. Boehm, J.; Heinkelmann, R.; Schuh, H. Short note: A global model of pressure and temperature for geodetic applications. *J. Geod.* **2007**, *81*, 679–683. [CrossRef]
28. Zhang, X.; Zhao, C.; Wang, Q.; Ma, Y. Carrier phase differential positioning augmented by LEO satellites. *Sci. Surv. Mapp.* **2017**, *42*, 14–18.
29. Teunissen, P.J.G. The least-squares ambiguity decorrelation adjustment: A method for fast GPS integer ambiguity estimation. *J. Geod.* **1995**, *70*, 65–82. [CrossRef]
30. Satellite Tool Kit, Analytical Graphics Incorporated, Exton, PA, USA. Available online: http://www.agi.com/products/stk/ (accessed on 21 January 2019).
31. DOD SPS, Department of Defense USA. Global Positioning System Standard Positioning Service Performance Standard, 4th Edition. 2008. Available online: http://www.gps.gov/technical/ps/2008-SPS-performancestandard (accessed on 6 January 2012).
32. Wang, J.; Feng, Y. Reliability of partial ambiguity fixing with multiple GNSS constellations. *J. Geod.* **2012**, *87*, 1–14. [CrossRef]